Effects of Permeant Ion Concentrations on the Gating of L-Type Ca^{2+} Channels in Hair Cells

Adrián Rodríguez-Contreras and Ebenezer N. Yamoah
Center for Neuroscience, Department of Otolaryngology, University of California at Davis, Davis, California 95616

ABSTRACT We determined the gating and permeation properties of single L-type Ca^{2+} channels, using hair cells and varying concentrations (5–70 mM) of the charge carriers Ba^{2+} and Ca^{2+}. The channels showed distinct gating modes with high- and low-open probability. The half-activation voltage ($V_{1/2}$) shifted in the hyperpolarizing direction from high to low permeant ion concentrations consistent with charge screening effects. However, the differences in the slope of the voltage shifts (in VM^{-1}) between Ca^{2+} (0.23) and Ba^{2+} (0.13), suggest that channel-ion interaction may also contribute to the gating of the channel. We examined the effect of mixtures of Ba^{2+} and Ca^{2+} on the activation curve. In 5 mM Ca^{2+}, the $V_{1/2}$ was, -26.4 ± 2.0 mV compared to Ba^{2+}, -34.7 ± 2.9 mV, as the charge carrier. However, addition of 1 mM Ba^{2+} in 4 mM Ca^{2+}, a molar ratio, which yielded an anomalous-mole fraction effect, was sufficient to shift the $V_{1/2}$ to -34.7 ± 1.5 mV. Although Ca^{2+}-dependent inactivation of the L-type channels in hair cells can yield the present findings, we provide evidence that the anomalous gating of the channel may stem from the closed interaction between ion permeation and gating.

INTRODUCTION

The primary functions of frog saccular hair cells are to sense, sort, and transmit relevant substrate-borne vibrations (Lewis et al., 1982). For rapid and precise transmission of behaviorally significant stimuli, hair cells employ voltage-gated Ca^{2+} channels that are poised to mediate neurotransmitter release at the hair cell-afferent nerve synapse. The dihydropyridine-sensitive L-type voltage-gated calcium channel (L-VGCC) is the predominant channel in hair cells (Zidanic and Fuchs, 1995; Kollmar et al., 1997a,b; Rodriguez-Contreras and Yamoah, 2001). The channel activates following a mechanically induced generator potential and allows Ca^{2+} entry, thereby mediating neurotransmitter release (Roberts et al., 1990; Fuchs, 1996; Moser and Beutner, 2000; Spassova et al., 2001). The influx of Ca^{2+} also activates Ca^{2+}-activated K^+ currents, which underlie resonance of the membrane potential (Crawford and Fettiplace, 1981; Ashmore, 1983; Lewis and Hudspeth, 1983; Armstrong and Roberts, 1998; Smotherman and Narins, 1999; Fettiplace and Fuchs, 1999).

The VGCC in hair cells belongs to the L-type Ca^{2+} channel class (Kollmar et al., 1997a,b). However, within this class, the hair cell L-VGCC exhibits three distinct properties: 1) The channels activate at a potential which is ~20 mV more negative than the threshold of activation of similar cardiac dihydropyridine-sensitive Ca^{2+} currents (Ohmori, 1984; Tsien et al., 1988; Art and Fettiplace, 1987; Hudspeth and Lewis, 1988a,b; Zidanic and Fuchs, 1995). 2) The current activates and deactivates rapidly (time constants ~0.5 ms). 3) The voltage- and current-dependent inactivation is slower than their cardiac counterparts (Lewis and Hudspeth, 1983; Fuchs et al., 1990; Zidanic and Fuchs, 1995). In a previous study, the properties of L-VGCC in hair cells were examined using varying concentrations of mostly Ba^{2+}, and at times, Na^+, as permeant ions to increase the magnitude of the whole-cell and single-channel currents (Art and Fettiplace, 1987; Art et al., 1995). The whole-cell Ca^{2+} current was evaluated with the implicit assumption that the total current was carried by the L-VGCC (Zidanic and Fuchs, 1995). Recently, several reports have demonstrated that although the predominant Ca^{2+} current is the L-VGCC, hair cells do express multiple Ca^{2+} channels that have distinct pharmacological and permeation properties (Su et al., 1995; Martini et al., 2000; Rodriguez-Contreras and Yamoah, 2001; Rodriguez-Contreras et al., 2002). Thus, single-channel recordings would be the most direct strategy to determine the properties of a single class of VGCC in hair cells.

Measurements of single Ca^{2+} channel currents have demonstrated that the unitary current magnitude and the conductance saturate at permeant ion concentrations above 20 mM, and thus, the sensitivity range of the channels lies between ~1–20 mM (Yue and Marban, 1990; Church and Stanley, 1996; Rodriguez-Contreras et al., 2002). Because the voltage-dependent kinetics of ion channels are remarkably affected by the species and concentration of the permeant ions (Zhou and Jones, 1995; Hille, 2001), we hypothesized that the gating of L-VGCC in hair cells would be altered at different concentrations of Ca^{2+}. By determining the kinetic properties of single L-type Ca^{2+} channels in hair cells, at concentrations within the dynamic range of the channel, the genuine features of the channel as Ca^{2+} transporters may then be elucidated.

In the present study, we determined the effects of permeant ions and their concentrations on the kinetic properties of L-VGCC in frog hair cells. We compared single-channel records of L-VGCC using varying concentrations of the charge carriers, Ba^{2+} and Ca^{2+}. Our results show that L-VG CCs in hair cells have different modes of gating as revealed by the use of different charge carriers. In addition, surface

Submitted October 8, 2002, and accepted for publication January 17, 2003.

Address reprint requests to Ebenezer N. Yamoah, University of California at Davis, Ctr. for Neuroscience, Dept. of Otolaryngology, 1544 Newton Court, Davis, CA 95616. Tel.: 530-754-6630; Fax: 530-54-7183/754-5046; E-mail: enyamoah@ucdavis.edu.

0006-3495/03/05/3457/13 $2.00

charge screening effects of divalent cations alone were insufficient to account for the voltage-dependent shifts of activation of the channel using varying ion concentrations. We propose that ion permeation and gating of the channel may be linked.

MATERIALS AND METHODS

Hair cell isolation

Hair cells were isolated as described previously (Yamoah et al., 1998). Frogs were sacrificed, using a protocol approved by the University of California, Davis, Animal Research Services, and inner ears were removed quickly and placed in oxygenated low-Ca^{2+} frog Ringer solution (in mM): 110 NaCl, 2 KCl, 3 D-glucose, 0.1 $CaCl_2$, and 5 *n*-2-hydroxyethylpiperazine-*n*′-2-2-ethanesulfonic acid (HEPES), pH 7.4 with NaOH. Macular tight junctions were disrupted by exposing the perilymphatic surface to 4 mM ethylene glycol-bis(β-aminoethyl ether)-*n*,*n*,*n*′,*n*′-tetraacetic acid (EGTA) for 15 min. After washing the preparation with fresh saline, the saccular macula was isolated and incubated in frog saline containing 50 μg/ml protease (type XXIV, Sigma Chemical, St. Louis, MO) for 20 min. The tissue was washed and transferred to frog saline containing 1 mg/ml bovine serum albumin (Sigma Chemical) and 2 mg/ml DNase I (Worthington, Lakewood, NJ) for 10 min. This procedure has been used previously (Chabbert, 1997) and differs from other more severe enzymatic treatments that can alter ionic conductances (Armstrong and Roberts, 1998). The otolithic membrane was excised and hair cells were dissociated from the macula using an eyelash. Hair cells were allowed to settle onto the bottom of the recording chamber (coated with the lectin concanavalin-A) for 20 min before patch-clamp recording.

Whole-cell current recordings

Whole-cell Ca^{2+} and Ba^{2+} currents were recorded from hair cells with length-to-apical diameter ratio (LAD) of ~4 that expressed predominantly L-type currents (Rodriguez-Contreras and Yamoah, 2001). The tips of the electrodes were filled with a solution containing (in mM) 130 CsCl, 5 HEPES (pH 7.3 with CsOH). To gain electrical access to the cell, electrodes were backfilled with solution containing (in mM) 130 CsCl, 1 $CaCl_2$, 5 HEPES, and amphotericin 200 μg/ml (pH 7.3 with CsOH; Rodriguez-Contreras and Yamoah, 2001). To ensure that recordings were in the perforated-patch mode instead of whole-cell mode, the backfilled solution of the patch electrode contained 1 mM Ca^{2+}. A switch from the perforated-patch to whole-cell mode resulted in rapid cell death because of Ca^{2+} toxicity. Series resistance (5–10 MΩ) was compensated (nominally 70–80%). Liquid-junction potentials were recorded and adjusted as described previously (Rodriguez-Contreras and Yamoah, 2001). Ca^{2+} currents were amplified with an Axopatch 200B amplifier (Axon Instruments, Foster City, CA). Outward K^+ currents were blocked with TEACl, 4-AP, and cesium (Cs^+) ions. Bath solutions contained (in mM) 90 NaCl, 25 TEA-Cl, 5 4-AP, 1.6-5 $CaCl_2$/$BaCl_2$, 3 glucose, and 5 HEPES (pH 7.4). Current records were filtered at 2–5 kHz with a low-pass Bessel filter and digitized at 10 kHz with a Digidata interface (Axon Instruments) controlled by custom-written software. Data were stored and analyzed in a personal computer.

Single-channel recording

The patch-clamp technique in the cell-attached configuration was used (Hamill et al., 1981). Patch pipettes were made from quartz glass using a horizontal laser puller (P-2000, Sutter Instruments, Novato, CA). Patch electrodes were filled with divalent cation solutions (in mM): 5-70 Ca^{2+} and Ba^{2+}, 20 tetraethyl ammonium chloride (TEACl), 5 4-aminopyridine (4-AP), 5 HEPES at pH 7.4 (adjusted with TEAOH). *N*-methyl-D-glucamine (NMG) was used to substitute for divalent cation and to maintain an osmolarity of ~280 mosmol. To identify the L-type channel, the experiments were conducted in the presence of the agonist Bay K 8644 (Calbiochem, La Jolla, CA) in the bath solution, which was applied after control current traces have been recorded. Stock solutions of Bay K 8644 (100 mM) were made in DMSO, and a final concentration of 5 μM was used. The bath solution contained (in mM): 80 KCl, 3 D-glucose, 20 TEACl, 0.2 $CaCl_2$, 5 4AP, 5 HEPES, and was adjusted to pH 7.4 with TEAOH, to shift the resting potential to ~0 mV. Using the external recording solutions, the resting membrane potential of hair cells was -0.4 ± 2.1 mV ($n = 32$; Rodriguez-Contreras and Yamoah, 2001). All other chemicals were obtained from Sigma. Experiments were carried out at room temperature (~21°C).

Single-channel currents were filtered at 1–2 kHz using a low-pass Bessel filter, sampled at 10–40 kHz, and stored in a personal computer. The channels were activated at a frequency of 0.2 Hz. Analysis was carried out using custom-written software, which was linked to Origin software (MicroCal, Northampton, MA). Leak and capacitative currents were corrected offline by fitting smooth templates to null traces and subtracting it from active traces. Open-close transitions were detected using half-height threshold analysis criteria. Idealized records were used to construct ensemble-averaged currents, open probability (P_o), and to generate histograms for the distributions of open and closed time intervals. P_o, voltage, and recording-time surface plots were generated using a built-in matrix function from Origin software (MicroCal). The time to reach the median of the cumulative first latency histograms was determined as described by Zei and Aldrich (1998). Unless indicated otherwise, all averaged and normalized data are presented as mean $\pm$ SD. The statistical significance of observed differences between groups of cells or between different parameters describing the properties of the currents were evaluated using a two-tailed Student's *t*-test; *p* values are presented in the text, and statistical significance was set at $p < 0.05$.

RESULTS

Ion-dependent kinetics of single L-type currents in hair cells

In our previous studies we showed that the sensitivity range of the L-type Ca^{2+} channel in hair cells lies between 1 and 20 mM of Ba^{2+} and Ca^{2+} (Rodriguez-Contreras et al., 2002). However, the gating properties of single L-type channel have been studied almost exclusively at saturating concentrations of Ba^{2+} or Ca^{2+} (Fox et al., 1987; Imredy and Yue, 1994; but see Smith et al., 1993). This section of the results compares the differences between the gating properties of the L-type channel using permeant ion concentrations at the dynamic (5 mM) and saturating (70 mM) levels. Fig. 1 shows characteristic cell-attached recordings of consecutive single L-VGCC current traces from isolated hair cells with 70 mM Ba^{2+} (Fig. 1 *A*) and Ca^{2+} (Fig. 1 *B*) as the charge carriers. Outward K^+ channel currents were blocked with TEA and 4-AP, and the cell membrane potential was artificially shifted to ~0 mV using high bath K^+ (80 mM; see Methods). The L-type channel was distinguished from the non-L-type channel by differences in the pharmacology of the two channels (Rodriguez-Contreras and Yamoah, 2001). Single-channel activity was recorded for ~4 min, and then the recording chamber was perfused with a high K^+ solution containing 5 μM Bay K 8644. Only patches with channels that showed increased long openings and had conductances that were consistent with L-type channels are presented in this report

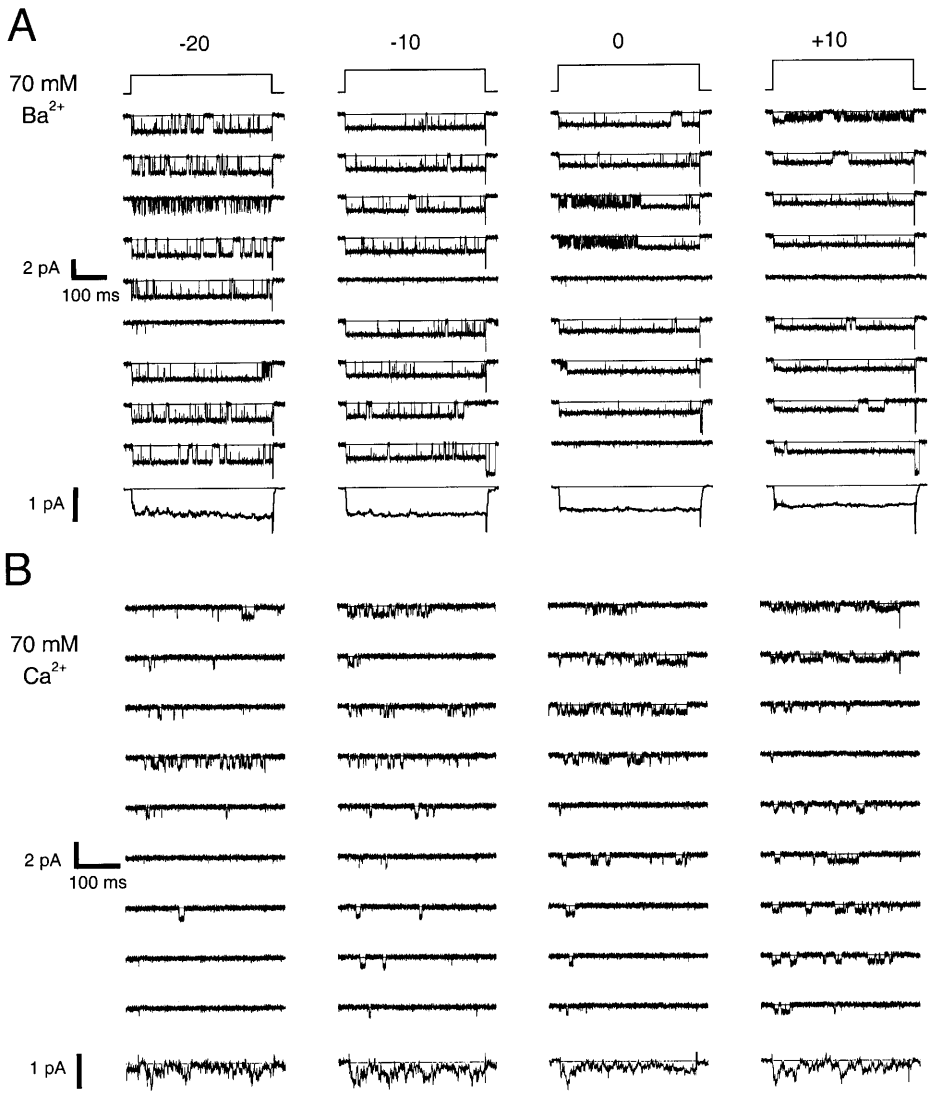

FIGURE 1 Single-channel currents in hair cells have ion-dependent kinetics. Representative single-channel traces of (*A*) Ba^{2+} and (*B*) Ca^{2+} currents at different test potentials were obtained from L-type channel using the agonist, Bay K 8644 (5 μM) in the bath solution. Nine consecutive traces are shown at the step potentials indicated, from a holding potential of −70 mV. The ensemble-averaged current traces derived from at least 200 consecutive sweeps are shown at the bottom of each column of traces. The kinetics of open events were described as fast or slow and as detailed in the text. Note that ensemble currents in *A* had a sustained time course, whereas ensemble currents in *B* showed a slowly decaying progression. In addition, openings at the end of the voltage step occurred more frequently in Ba^{2+} than Ca^{2+} currents.

(Rodriguez-Contreras and Yamoah, 2001; Rodriguez-Contreras et al., 2002). Patch depolarization from a holding potential of −70 mV to step potentials between −20 and +10 mV are shown. A close inspection of the Ba^{2+} current traces reveals short and long openings as well as brief and long closures. In addition, the gating of the channel included periods of quiescence. The patch contained only one channel, as there was no stacking of events. Furthermore, direct transitions from fast to slow kinetics with similar current amplitude, and vice versa, were observed in these recordings, indicating that these gating modes were derived from a single channel. The Ba^{2+} currents also showed frequent re-openings upon membrane repolarization, which were readily visible in the ensemble-averaged currents that showed well-resolved tail currents. The Ca^{2+} current had infrequent openings but the brief and long event characteristics persisted. However, when compared to Ba^{2+} currents, there was an increased frequency of closures (Fig. 1 *B*). The ensemble-averaged Ca^{2+} currents showed a slow decay, which is in sharp contrast to the sustained Ba^{2+} currents as shown in Fig. 1 *A* (also see Fig. 5). Furthermore, compared to Ba^{2+} single-channel fluctuations, the probability of openings significantly decreased when Ca^{2+} was the charge carrier ($p < 0.05$), and the long closures dominated the unitary Ca^{2+} current traces (Fig. 1 *B*).

The single-channel current traces in Fig. 1 were recorded at charge carrier concentrations where the unitary current and conductance were fully saturated. Although physiological saline contains ~1.6 mM Ca^{2+}, the signal-to-noise ratio of the unitary Ca^{2+} currents recorded under these conditions was low and not suitable for detailed kinetic analyses (Rodriguez-Contreras and Yamoah, 2001). Since the apparent dissociation constant (K_D) of the channel is ~5 mM (Rodriguez-Contreras et al., 2002), we crosschecked the properties of the Ca^{2+} channels using 1.6 versus 5 mM charge carrier. Shown in Fig. 2 are whole-cell Ca^{2+} (Fig. 2 *A*) and Ba^{2+} (Fig. 2 *B*) current traces measured using 1.6 and 5 mM of the charge carriers. The corresponding current-voltage relationship is shown in Fig. 2 *C*. The steady-state activation of whole-cell

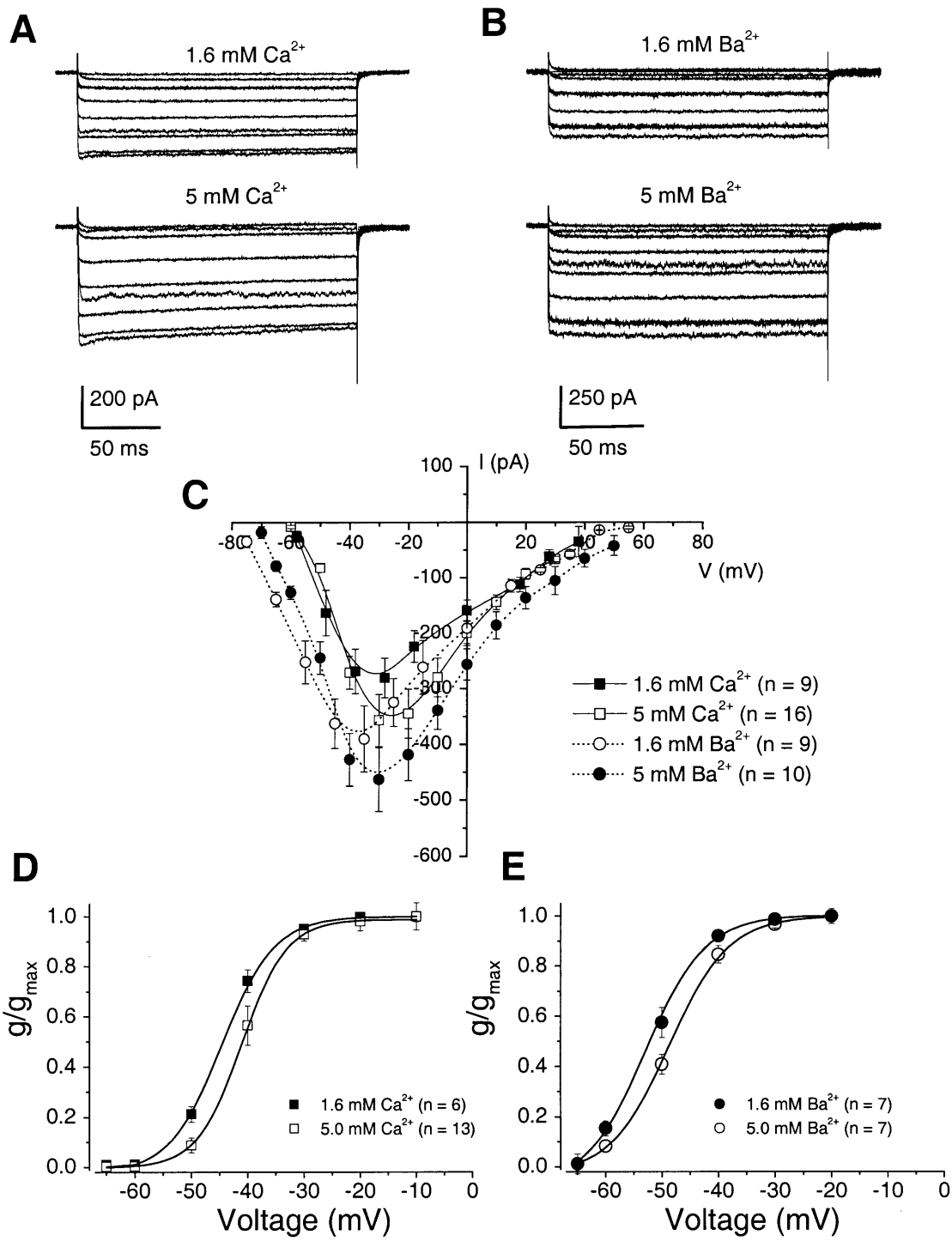

FIGURE 2 Voltage-dependent activation of whole-cell Ca^{2+} currents in hair cells shifted slightly to the right using (in mM) 1.6 versus 5.0 of the charge carrier. (*A* and *B*) Family of Ca^{2+} (*A*) and Ba^{2+} (*B*) current traces obtained from hair cells with length-to-apical diameter ratio ~4. The corresponding current-voltage (I-V) relationship is shown in *C*. The conductance of whole-cell Ca^{2+} currents was normalized and plotted against the step potential. The conductance of the current was determined using the estimated reversal potential of the current from the I-V curve and the step potential to calculate the electrical driving force. Error bar represents mean ± SE. Continuous curves were generated from the Boltzmann function $g/g_{max} = \{1 + \exp(V_{1/2} - V)/k_m]\}^{-1}$, where $V_{1/2}$ is the half-activation voltage, k_m is the maximum slope, g is the conductance of the current, and g_{max} denotes the maximum conductance. The reversal potentials were derived from the current-voltage relationship plots (*C*). The values of $V_{1/2}$ and k_m obtained from the activation curves for whole-cell current in 1.6 and 5 mM Ca^{2+} solutions were -44.9 ± 0.4 mV ($n = 6$), -41.4 ± 1.4 mV ($n = 13$), and 4.7 ± 0.5 mV and 4.1 ± 1.0 mV, respectively. (*D*) Similar analyses were performed using data collected from experiments when 1.6 and 5 mM Ba^{2+} was the charge carrier for whole-cell currents. The values of $V_{1/2}$ and k_m obtained from the activation curves for whole cell current in 1.6 and 5 mM Ba^{2+} solutions were -51.3 ± 2.2 mV ($n = 7$), -48.6 ± 1.1 mV ($n = 7$), and 4.5 ± 1.1 mV and 4.7 ± 1.0 mV, respectively.

Ca^{2+} currents in hair cells, which expressed mostly the L-type current (see Methods), was also examined. The rightward shift in the steady-state activation curve, as external Ca^{2+} (1.6 mM) and Ba^{2+} (1.6 mM) were increased to 5 mM, was modest (Fig. 2, *D* and *E*), providing credible assurance that 5 mM Ca^{2+} or Ba^{2+} would be a reasonable concentration to determine the kinetics of the Ca^{2+} channel.

Fig. 3 shows representative recordings from single L-type Ca^{2+} channels using 5 mM Ba^{2+} and Ca^{2+} as the charge carriers. Ba^{2+} currents showed single-channel kinetics that were similar to those described in Fig. 1 *A*. For traces where there were channel openings, the P_o was higher in 5 mM than when the permeant ion concentration was 70 mM (Fig. 3 *B*). However, there were more null traces in recordings using low (5 mM) permeant ion concentrations. Thus, the resulting mean P_o was similar at the two different concentrations (Fig. 1 *B*). One of the noticeable features of the L-VGCC was that the mean P_o was less than 1 even in the presence of an agonist, Bay K 8644, implying the existence of absorbing closed states (see Fig. 6). Variations in the mean P_o using different ions and concentrations further suggested that the dwell time in the closed states might be ion- and concentration-dependent.

Contour maps of P_o, time, and test potentials were generated to provide graphic analyses of the charge carrier and concentration-dependence on the gating of the channel. Fig. 4 shows surface plots of the P_o at different times and membrane potentials for representative recordings at charge carrier concentrations of 70 mM and 5 mM. The P_o of the channel was voltage- and time-dependent. Although there were differences in the modal gating of the channel in 70 mM versus 5 mM Ba^{2+}, they were not as striking as between high and low concentrations of Ca^{2+}. In general, for a given step potential, the P_o increased with decreased concentration as a result of increased long openings and a decline in closures. However, there was an increased propensity for the channel to enter into quiescent modes as well. These results are similar to that reported for L-type Ca^{2+} channels in hippocampal neurons (Thibault et al., 1993).

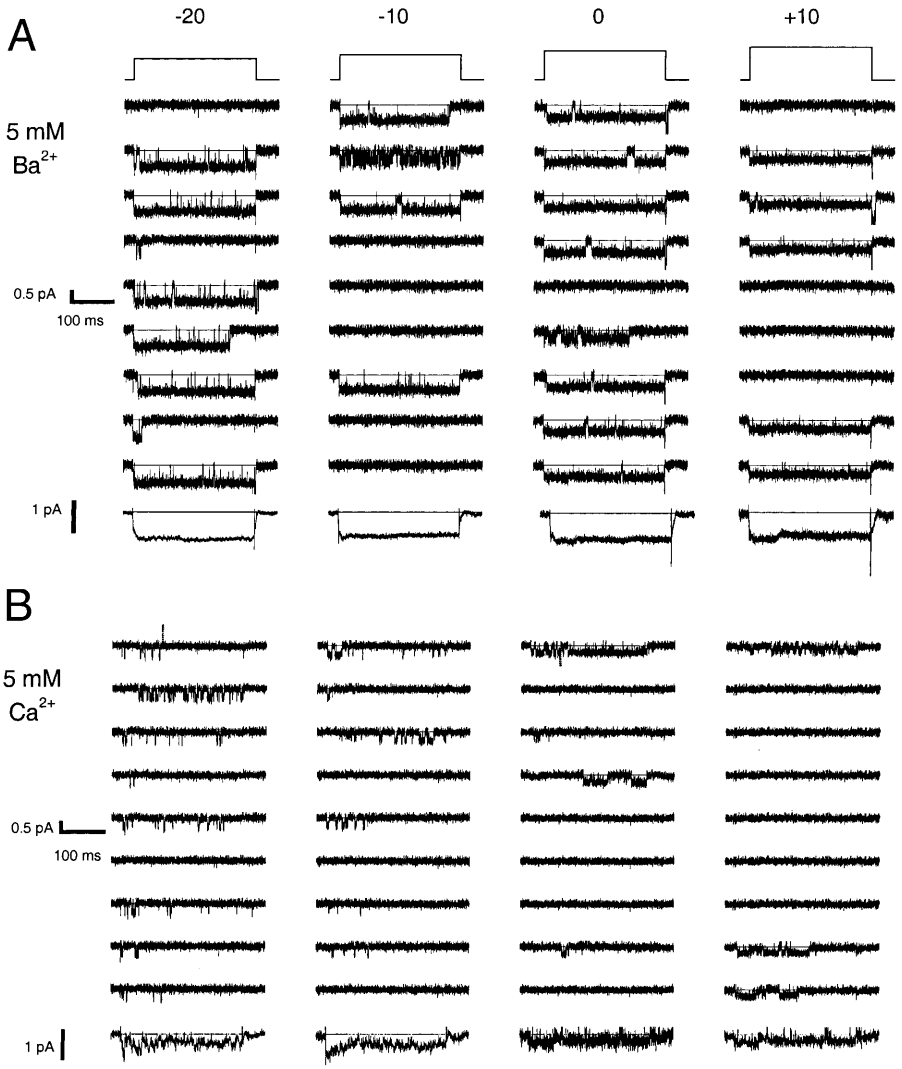

FIGURE 3 Single-channel current fluctuations were evident using 5 mM divalent cations charge carrier. Characteristic traces of Ba^{2+} (*A*) and Ca^{2+} (*B*) currents at different test potentials were obtained as described in Fig. 1, except that the concentration of divalent cations in the pipette solution was 5 mM. Ensemble-averaged currents, shown below each column of single-channel sweeps, were derived from ~100 consecutive sweeps. The contribution of blank sweeps in *B* is seen in the noise and decay of the ensemble-averaged currents. Finally, channel openings at the end of the depolarizing step were observed in current recordings shown in *A*, but were rare in *B*. Thus, the tail currents in the ensemble-averaged current traces were well resolved in Ba^{2+} but not in Ca^{2+} currents.

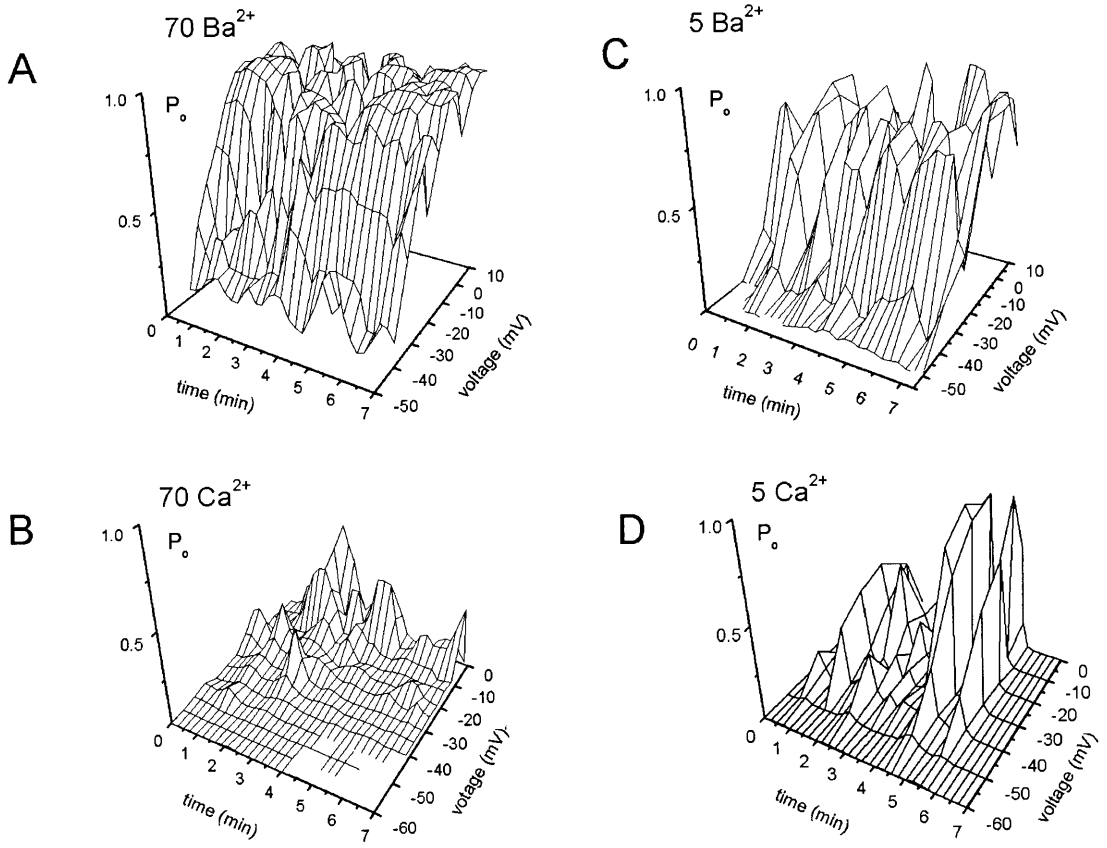

FIGURE 4 The species and concentration of divalent cations reveal modal gating of L-type channel currents in hair cells. The relationship between the P_o values, step voltage, and time is shown for Ba^{2+} and Ca^{2+} current recorded at 70 (*A* and *B*) and 5 mM (*C* and *D*). The contour plots of P_o, voltage, and time were generated from consecutive unitary current fluctuations. Only the first 7 min of recordings are shown for clarity of presentation. Ba^{2+} currents had similar surface plots at 70 and 5 mM (*A* and *C*), while the activation voltages differed. For Ca^{2+} currents at 5 mM, there were frequent long openings, which were interrupted with long closures and null sweeps.

Inactivation of single L-type channel currents

Ensemble-averaged current traces derived from more than 500 sweeps of single-channel traces revealed that the channel showed a slow decay when Ca^{2+} was the charge carrier (Fig. 5, *A* and *B*). In contrast, in the presence of Ba^{2+} as charge carrier, the ensemble-averaged current was virtually sustained (Fig. 5, *C* and *D*). As shown in Fig. 5 *E*, the degree of inactivation was enhanced in 70 versus 5 mM Ca^{2+}, and was also increased at step voltages where the maximum current was recorded, suggesting that the decay of the current was dependent on Ca^{2+}.

Concentration-dependent shift in the activation of single L-type channel currents

The effect of charge carrier concentration on the activation of L-VGCC was assessed from the P_o versus voltage plots shown in Fig. 6, where the solid lines represent fits to the Boltzmann function. Although the data were derived from Bay K 8644-treated channels, the open-probability of the channels was invariably less than 1 (Fig. 6, *A* and *B*). For comparisons of the activation curves, the data in Fig. 7, *A* and *B*, have been normalized. Whereas the activation threshold of the channel was ~ -50 mV and the half-activation voltage ($V_{1/2}$) was ~ -30 mV for 70 mM Ba^{2+} currents, the activation voltage and $V_{1/2}$ for Ca^{2+} currents were ~ -45 and -10 mV, respectively. Moreover, the slope factor (k) for current carried by the two ions remained fairly constant ($\sim$5 mV). The effects of reduced concentrations (5 mM) of permeant ions were modest compared to the predicted decline in the surface charge screening of divalent cations (Zhou and Jones, 1995). The $V_{1/2}$ of Ca^{2+} current shifted by $\sim$16 mV in the hyperpolarizing direction (Fig. 7, *B* and *C*). By contrast, the negative potential shift of the $V_{1/2}$ for 5 mM-Ba^{2+} current was fairly small ($\sim$7 mV). In sharp contrast to the observed shifts in the activation curves, if one assumes that there were no binding of the permeant ions to the surface charge, a voltage shift of $\sim$25 mV is expected from a 70 to 5 mM drop in divalent ion concentration (Zhou and Jones, 1995; Zamponi and Snutch, 1996). Further, the slope factors (in VM^{-1}) were 0.23 and 0.13 for Ca^{2+} and Ba^{2+}, respectively, representing an approximate twofold difference between these ions (Fig. 7 *C*).

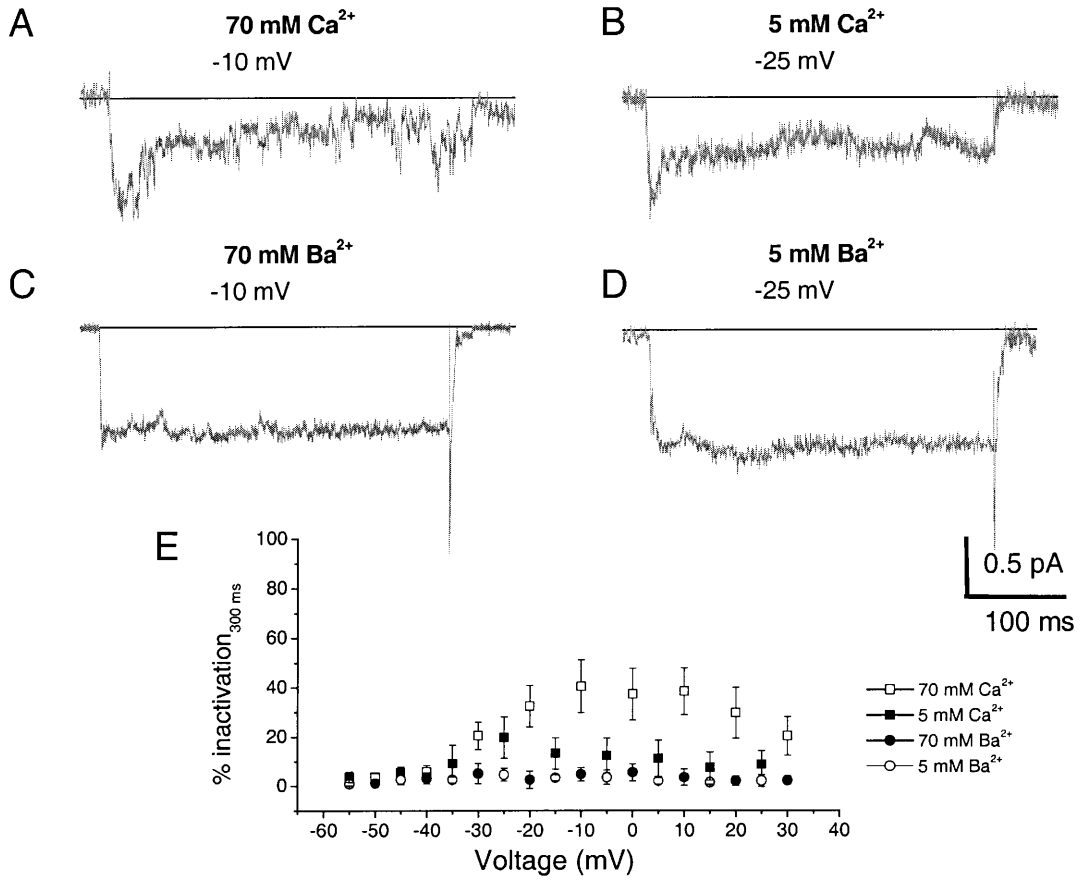

FIGURE 5 Effects of Ca^{2+} and Ba^{2+} on the profile of ensemble-averaged currents of single L-type channels. Ca^{2+} caused a relatively slow relaxation of the ensemble-averaged currents, which was more pronounced in 70 mM (*A*) than in 5 mM (*B*). Cell-attached patches containing single-channel currents were held at a holding potential of −70 mV and stepped to the potentials indicated beside the traces. The ensemble-averaged currents were generated from 530 consecutive single-channel traces. The decay of the ensemble-averaged currents was virtually abolished when Ba^{2+} was used as the charged carrier (*C* and *D*). (*E*) The degree of inactivation (expressed as percentage of inactivation) was determined at 300 ms and plotted against the step voltage. Data were generated from ensemble-averaged currents, which were recorded from single-channel traces (>500 sweeps each), obtained from six patches for the four different experimental conditions.

To test the prediction that ion-channel interaction in the permeation pathway may influence the shift in $V_{1/2}$, we examined the effects of mixtures of Ca^{2+} and Ba^{2+} on the activation curves (Fig. 8). The inclusion of 1 mM Ba^{2+} in a Ca^{2+}:Ba^{2+} ratio of 4:1 was sufficient to shift the activation curve to that of 5 mM Ba^{2+} alone (shown in *dotted line* in Fig. 8 *A* and as group data in Fig. 8 *B*). This underpins the notion that ion permeation may contribute toward the voltage-dependent activation of the channel. Furthermore, we have previously demonstrated that a mole fraction of 4:1 for Ca^{2+}:Ba^{2+} produces a robust anomalous mole fraction effect on the L-VGCCs (Rodriguez-Contreras et al., 2002). Taken together, these data suggest that ion permeation is linked tightly to the gating of the channel. Alternatively, if one of the permeant ion increases the tendency of the channel to enter into a nonconducting state, then the P_o at any given step voltage is expected to be low for that ion, and should shift the activation curve to the right. Thus, Ca^{2+}-dependent inactivation of the channel can potentially yield the present findings as well (Imredy and Yue, 1994).

Latencies to first openings of the L-VGCC

The distribution of the first latency or the waiting times of the channel provides an index on whether it has single or multiple closed states, and on the degree of reluctance of transition between closed to open states (Imredy and Yue, 1994). The appearance of multiple null sweeps as shown in Figs. 1 and 3 ruled out the possibility that the L-VGCC exhibited a single closed state. The normalized cumulative first latency distributions was voltage-dependent as shown in Fig. 9 *A*, which suggested that the contribution of transitions before first openings to the voltage-dependence of channel activation, and the time to reach the median first latency should decrease with increasing membrane depolarization (Zei and Aldrich, 1998). For a channel that exhibits Ca^{2+}-dependent

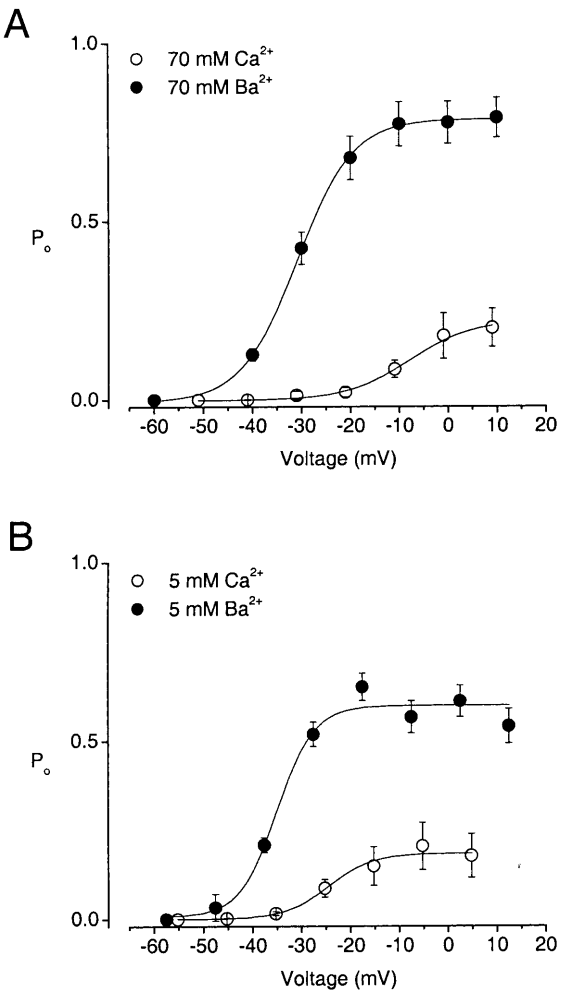

FIGURE 6 A shift in the activation of L-type currents is dependent on the concentration and species of charge carrier. Open probability of divalent cation currents are shown. Mean P_o values of recordings from single-channel patches stepped to varying potentials were determined as described in the methods section for Ba^{2+} (●) and Ca^{2+} (○) current at 70 (*A*) and 5 mM (*B*). The P_o was determined from consecutive depolarizing steps to different potentials as described in Figs. 1 and 2. The frequency of unitary current openings was higher in Ba^{2+} than in Ca^{2+}. The maximum P_o (P_{omax}) in Ba^{2+} was 0.71 ± 0.11 ($n = 11$) and 0.60 ± 0.10 ($n = 9$) at 70 and 5 mM, respectively, and the corresponding P_{omax} in Ca^{2+} was 0.20 ± 0.10 ($n = 9$) and 0.24 ± 0.12 ($n = 10$) at 70 and 5 mM, respectively.

inactivation (see Fig. 5), we expected that the first latency distribution would be faster in Ba^{2+} than in Ca^{2+}. Fig. 9 *B* depicts the time course of the first latency distribution of the channel in 5 mM Ca^{2+} and Ba^{2+}. Using charge carrier concentrations (in mM) of 4 Ca^{2+} and 1 Ba^{2+}, the first latency distribution became brief when compared to Ca^{2+} alone, and shifted toward the distribution produced by 5 mM Ba^{2+} (Fig. 9, *B* and *C*). However, the median of the first latency distribution decayed exponentially with voltage as shown in Fig. 9 *C*. Furthermore, the leftward shift in the curve as the charge carrier was changed from 5 mM Ca^{2+} to Ba^{2+} indicated that at least one of the transition rates from the closed states before first opening may be altered by the permeant ion.

DISCUSSION

In this study, we provide the first description of the gating properties of L-type VGCC at the single-channel level in hair cells. The charge carriers and its various concentrations sculpt the gating mechanisms of the L-type channel. The main effect of increasing the charge carrier concentration was to shift the activation of L-VGCC currents to depolarizing potentials. Such effect is consistent with screening of surface charges by divalent cations. However, the magnitude of the shift from 70 mM to 5 mM Ba^{2+} was notably smaller than that observed with Ca^{2+}, signifying that ion-ion and ion-channel interactions may influence the gating kinetics of the L-VGCC. At 5 mM, single-channel Ca^{2+} currents activated at potentials ~7 mV more positive than Ba^{2+} currents. However, in mixtures of Ca^{2+} and Ba^{2+} ions (molar ratio, 4:1), L-VGCC currents had activation profiles similar to those of Ba^{2+} currents, indicating that the interactions between the charge carriers and the channel shape the kinetics of the currents. Overall, we propose that ion-channel interactions involving the permeation pathway are able to modify the gating properties of single L-VGCC in hair cells.

Several inferences that are independent of any model-based predictions of the gating and permeation properties of single L-VGCC in hair cells can be made from the present study. These include: 1), The activation and deactivation kinetics, as assessed from the ensemble-averaged currents, were exceedingly fast (<300 μs). This is in sharp contrast to the relatively slow kinetics of the L-type channels in cardiac myocytes and sensory neurons (Fox et al., 1987; Tsien et al., 1988). The activation time constants were similar to those obtained for L-type channels in mouse pancreatic β-cells (Smith et al., 1993), and was consistent with the findings that hair cells and pancreatic β-cells express the L-type channel variety of $Ca_V1.3$ (Kollmar et al., 1997a; Ertel et al., 2000; Rodriguez-Contreras and Yamoah 2001). 2), Multiple closed states of the channel are traversed from the resting to at least two kinetically discernible open states via voltage-dependent transitions, similar to those in K^+ channels (Hess et al., 1986; Zagotta et al., 1994; Zei and Aldrich, 1998). Using an extension of the Hodgkin and Huxley (1952) formalism for ionic conductances, previous reports described the activation state variable (m) of the whole cell Ca^{2+} current in hair cells with a second-order function (m^2; Hudspeth and Lewis, 1988b; Zidanic and Fuchs, 1995). This is consistent with the observation that L-type channels in hair cells have more than one closed state. Furthermore, a significant number of studies on the kinetics of single Ca^{2+} channel gating have been carried out using 110 mM Ba^{2+} as the charge carrier to increase the current amplitude. Since the proportion of channels in the different closed states and the dwell times of the open states vary from high to low concentrations of the permeant ions, such conditions do not reveal the true features of the channel as a Ca^{2+} transporter. 3), Because there was no marked shift in the activation curve for currents recorded in

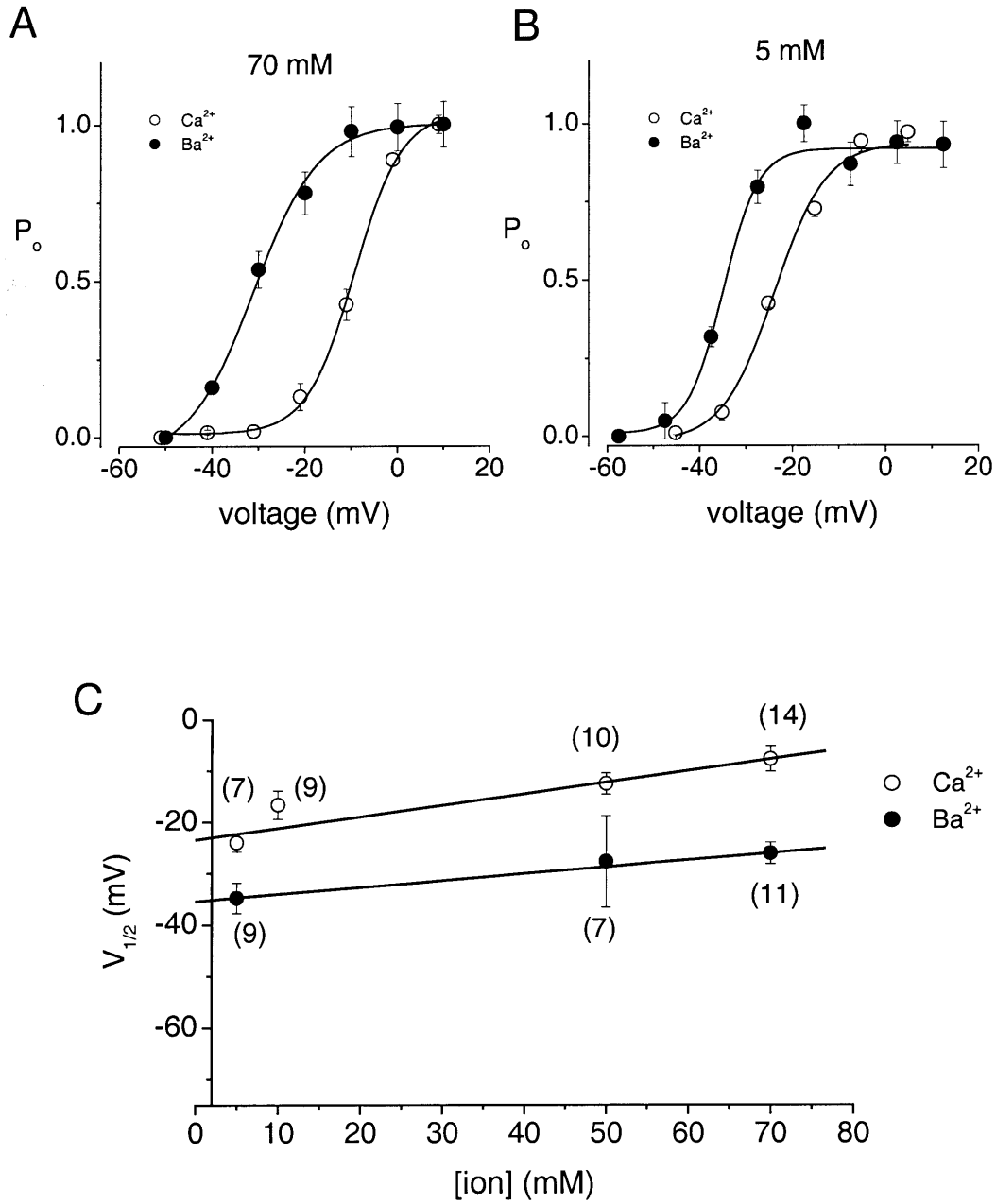

FIGURE 7 Voltage-dependent activation of the Ca^{2+} channel shifted leftward from high to low concentrations of permeant ions. Plots of normalized P_o versus voltage compare the extent of shift of the voltage-dependent activation of single-channel currents in hair cells at 70 and 5 mM Ba^{2+} (*A*) and Ca^{2+} (*B*). The data were fitted with the Boltzmann function. The $V_{1/2}$ and K_m were as follows: 70 mM Ba^{2+}, -28.0 ± 4.0 mV, and 6.0 ± 1.1 mV; 70 mM Ca^{2+}, -7.6 ± 2.5 mV, and $5.0 + 0.6$ mV; 5 mM Ba^{2+}, -35.0 ± 1.0 mV, and 4.5 ± 1.0 mV; 5 mM Ca^{2+}, -24 ± 1.8 mV, and 5.4 ± 2.0 mV ($n = 9$), respectively. Whereas the activation curve shifted by ~7 mV when Ba^{2+} was the charge carrier, the curve shifted by ~16 mV when Ca^{2+} was the permeant ion. (*C*) $V_{1/2}$ values were plotted at different ion concentrations to compare the shift in activation using different charge carriers. The slope of the regression lines were 0.23 ± 0.06 VM^{-1} and $0.13 + 0.01$ VM^{-1} for Ca^{2+} and Ba^{2+}, respectively. Numbers in parentheses represent the number of cells.

1.6 versus 5 mM divalent cations, and because the single-channel currents were better resolved in the latter, 5 mM appears to be a suitable experimental concentration to study the kinetics of Ca^{2+} channels. Still, the present findings may fall short of revealing the physiological properties of the channel, since the current analyses were performed on a Bay K8644-modified channel. It would be interesting to use a gating modifier, such as kurtoxin, to determine whether these findings persist (Sidach and Mintz, 2002). 4), The L-VGCC in hair cells displays weak Ca^{2+}-dependent inactivation. The modest inactivation and the increased occurrence of null sweeps necessitates the inclusion of an absorbing closed state, where the channel switches reluctantly toward openings (Imredy and Yue, 1994). Moreover, Ca^{2+} may favor some of

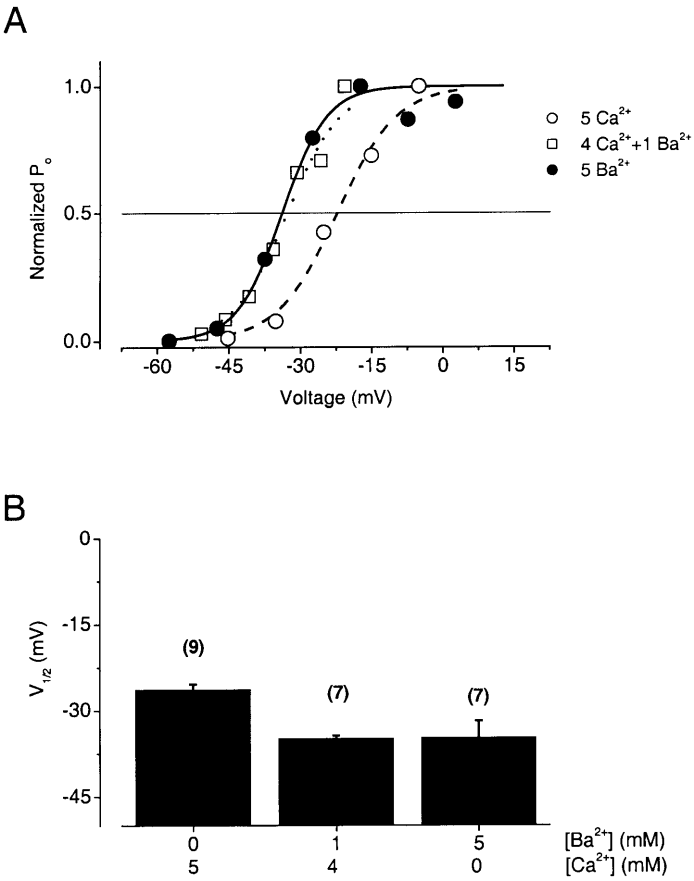

FIGURE 8 Plots of the voltage-dependent activation of unitary currents from the L-type channels in mixtures of Ca^{2+} and Ba^{2+} show the extent of shift. The total concentration of permeant ions, Ba^{2+} and Ca^{2+} was 5 mM. (*A*) Representative data for the activation of currents carried by Ca^{2+} (○), Ba^{2+} (●), and a mixture of Ca^{2+} and Ba^{2+} (□, molar ratio 4:1). The half-activation potentials ($V_{1/2}$) and the slope factor, *k*, for the examples shown are: (Ba^{2+}:Ca^{2+} ratio, 5:0) −34.8 mV and 4.5 mV (Ba^{2+}:Ca^{2+} ratio, 0:5); −23.2 mV and 6.7 mV, and (Ba^{2+}:Ca^{2+} ratio, 1:4) −32.9 mV and 7.0 mV. The data were obtained from three different cells. (*B*) Bar plots of the $V_{1/2}$ and the molar ratio of Ba^{2+} and Ca^{2+} are shown, where the number of patches (*n*), are indicated in parentheses. The mean $V_{1/2}$ were (Ba^{2+}:Ca^{2+}): 5:0 = −34.7 ± 2.9 mV; 1:4 = 34.7 ± 1.5 mV; and 0:5 = −26.4 ± 2.0 mV. The activation curve of single L-type channels in the mixture of Ba^{2+}/Ca^{2+} at molar ratio of 1:4 is very similar to Ba^{2+}-alone solution.

the nonconducting state since Ba^{2+} currents do not exhibit pronounced inactivation. Previous studies on hair cell Ca^{2+} currents have shown the absence of a voltage-dependent inactivation mechanism (Zidanic and Fuchs, 1995), and a weak Ca^{2+}-dependent inactivation process (Ohmori, 1984; Armstrong and Roberts, 1998; Smothermann and Narins, 1999; Platzer et al., 2000; Martini et al., 2000). Our present results demonstrate the presence of a Ca^{2+}-dependent inactivation of the dihydropyridine-sensitive Ca^{2+} channels. The existence of a clear inactivation from the ensemble-averaged Ca^{2+} current traces generated from single-channel patches, implies that the inactivation observed at the whole-cell level may be a genuine biological phenomenon. Because the inactivation of the L-type Ca^{2+} current in hair cells is slow, long-duration stimuli may be required to study the phenomenon in detail. Thus, the apparent lack of strong inactivation in the whole-cell current traces (Fig. 2 *A*) as compared to the ensemble-averaged current (Fig. 5 *B*) may stem from varying stimulus protocols that were employed to elicit the current. Alternatively, the ω-shaped configuration of cell-attached patches may have dislodged the channels from synaptic proteins, which may impede the inactivation of the channel (Song et al., 2003). And 5), For the L-VGCC current in hair cells, ion permeation and gating may be linked closely. The molar ratio of Ba^{2+}:Ca^{2+} mixtures that produced robust anomalous mole fraction effects in the channels' conductance (Rodriguez-Contreras et al., 2002) also showed striking alterations in the voltage-dependent activation of the current. Ca^{2+} was the predominant ion in a 4:1 ratio (Ca^{2+}:Ba^{2+}) solution, and thus, it is unlikely that Ca^{2+}-dependent inactivation plays a dominant role in the shifts in first latency distribution curves. Therefore, Ca^{2+}-dependent inactivation of the channel would be an unlikely explanation for the shift in first latency distribution as well as the activation curves described earlier, using the mole fraction of 4:1 (Ca^{2+}:Ba^{2+}). Instead, the data support the notion that permeation and gating are linked.

In a previous study of the kinetics of VGCC in hair cells, four properties of the channel were found (Zidanic and Fuchs, 1995): 1), low efficacy of current blockade by dihydropyridine antagonists; 2), low threshold of activation; 3), rapid kinetics of activation/deactivation; and 4), lack of current- and voltage-dependent inactivation. The cloning of a $Ca_{V1.3}$ subunit from the chick basilar papillae and the identification of alternative spliced variants in the same tissue (Kollmar et al., 1997a,b) may provide an explanation for the unique features of the L-type VGCC in hair cells. Moreover, studies of native channels at the whole cell and single-channel levels have shown that hair cells express different types of VGCC (Su et al., 1995; Martini et al., 2000; Rodriguez-Contreras and Yamoah, 2001; Rodriguez-Contreras et al., 2002). Whereas the expression of multiple Ca^{2+} channels may explain the incomplete block by

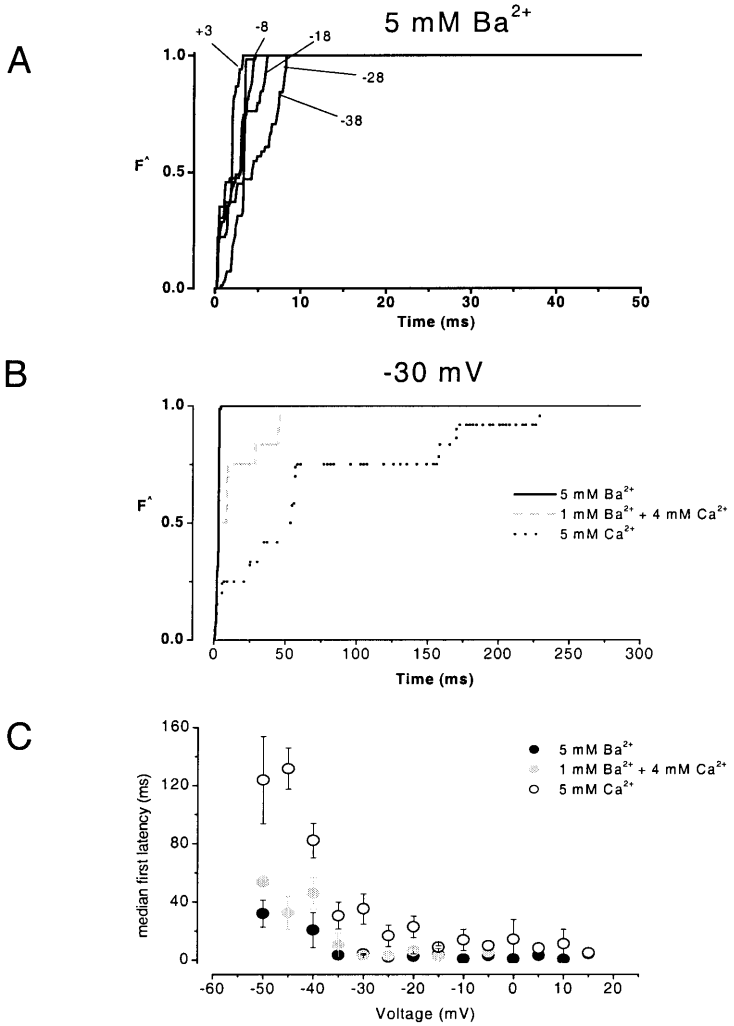

FIGURE 9 Voltage-dependence of first latency distribution in single-channel Ba^{2+} currents is shown. Cumulative first latency distribution plots were generated from the waiting time to first opening as a function of time, at the step voltages indicated. (*A*) shows the normalized first latency distribution (F′) of single-channel currents recorded using 5 mM Ba^{2+} as the charge carrier. (*B*) compares F′, which were generated at a step potential of −30 mV from a holding potential of −70 mV using the mole ratio of Ba^{2+}:Ca^{2+}, 5:0 (*solid line*), 1:4 (*dashed line*), and 0:5 (*dotted line*). The time to reach the median of the first latency at different potentials is shown in *C*. The times to reach the median of the first latency were distinct at negative voltages (−50 to −10 mV; $n = 7$).

dihydropyridines, we have demonstrated that the effects of voltage-dependent block of the dihydropyridines can also contribute toward the apparent weak sensitivity of hair-cell Ca^{2+} currents to the drug (Rodriguez-Contreras and Yamoah, 2001). Heterologous expression of $Ca_{V1.3}$ in mammalian cell lines has demonstrated that the ensuing current was less sensitive to nimodipine and nifedipine (Koschak et al., 2001; Safa et al., 2001; Song et al., 2003; Xu and Lipscombe, 2001). Although the expression of the α_1 subunit of L-type channel has provided traces of the properties of the L-type current in hair cells, the contribution of auxiliary subunits of the channel may be required to confer the native current phenotype (Song et al., 2003). In addition, emerging evidence suggest that synaptic proteins may also modulate the α_1 subunit to confer native channel properties (Song et al., 2003).

Effects of charge carriers and concentrations on the properties of L-VGCC currents

The permeation and gating properties of VGCC depend on the species and concentration of ions (Hille, 2001). The screening of negative surface charges by divalent cations alters the surface potential, which in turn affects the gating properties of the channels (Hille, 2001; Zhou and Jones, 1995). This is consistent with the results shown in Figs. 6 and 7, since the $V_{1/2}$ is proportional to the increase in ion concentration. Similar reports have been presented for L-type VGCC in pancreatic β-cells (Smith et al., 1993), in other native Ca^{2+} channels (Hagiwara and Ohmori, 1982), and in heterologous systems expressing different VGCC subunits (Mangoni et al., 1997; McNaughton and Randall, 1997; Wakamori et al., 1998). Moreover, our findings demonstrate that the species of the permeant ion determine the magnitude of the shift in the voltage-dependent activation. If charge screening were the only factor determining the effects on gating properties, we expected that different kinetic components of L-VGCC currents would be affected equally by the increase in charge carrier concentration. However, this was not the case in the present study. An alternative explanation for the effects of charge carriers on the gating properties of L-type VGCC would be the role of ion-channel interactions. Increasing the concentration of charge carriers has a direct effect on the permeation properties of VGCC, as observed by the saturation of single-channel current amplitude or conductance (Guia et al., 2001;

Church and Stanley, 1996; Smith et al., 1993; Zhou and Jones, 1995). We have shown previously that hair cell L-type channel conductance saturates with a K_D ~5 mM (Rodríguez-Contreras et al., 2002), a value consistent with various studies on unitary L-type currents (Church and Stanley, 1996; Smith et al., 1993). In addition, the properties of L-type VGCC in the concentration range of 2–5 mM are distinct compared to the properties of the channel at higher concentrations (Rodriguez-Contreras et al., 2002). The data presented in Fig. 8 suggest that interaction of ions and the channel may have direct effects on the kinetics of L-type VGCC, thereby affecting the activation of the unitary currents.

A nonpermeant ion, NMG, was used to substitute for Ba^{2+} and Ca^{2+} under 5 mM permeant ion conditions. Zhou and Jones (1995) showed that NMG may produce partial blockade of Ca^{2+} channels, which would provide an alternative explanation for the change in gating kinetics observed in our study. However, the maximal concentration of NMG used in this study is much smaller (65 mM) than the reported IC_{50} of NMG (300 mM; Zhou and Jones, 1995). The ~5–10% block of the channel is insufficient to explain our findings. Thus, it is unlikely that the results obtained in this study can be attributed to the blocking effects of NMG.

Functional implications for hair cells

The findings that the probability of channel openings increases with decreasing concentrations of Ca^{2+} is reminiscent of previous data from hippocampal neurons, where membrane repolarization-induced openings of the L-type Ca^{2+} channel may confer Ca^{2+}-dependent afterhyperpolarization (Thibault et al., 1993). In hair cells, this phenomenon would be essential for sustaining membrane oscillation and preventing excessive hyperpolarization induced by multiple outward K^+ currents. A common feature among vertebrate hair cells is the presence of small amplitude voltage-gated Ca^{2+} currents (Art and Fettiplace, 1987; Fuchs et al., 1990; Lang and Correia, 1989; Lewis and Hudspeth, 1983; Masetto et al., 2000; Nakagawa et al., 1991; Ohmori, 1984; Platzer et al., 2000; Smotherman and Narins, 1999), wherein the kinetic properties have been evaluated previously at the whole cell level (Hudspeth and Lewis, 1988a; Ohmori, 1984; Zidanic and Fuchs, 1995). Implicit in such analysis is the assumption that there is a homogeneous population of VGCC, an assumption which is not supported by recent evidence showing the presence of multiple VGCC in vertebrate hair cells (Su et al., 1995; Martini et al., 2000; Rodriguez-Contreras and Yamoah, 2001). In addition, previous studies used relatively higher concentrations of charge carriers to measure the current (Ohmori, 1984; Zidanic and Fuchs, 1995). By comparing the kinetic profiles of Ca^{2+} and Ba^{2+} currents at the single-channel level, we obtained qualitative results that allow inference of the properties of L-VGCC as physiological Ca^{2+} transporters. First, the species of charge carrier determines the P_o of the channels with the P_o being larger for Ba^{2+} than for Ca^{2+}. This suggests that the functional impact of Ca^{2+} domain formation in hair cells may be determined by the number of VGCCs that are in close proximity to each other (Roberts et al., 1990), or, by the relative distance of the channels to the Ca^{2+} binding sites (Hall et al., 1997). Second, crucial differences were observed between the time-dependent properties of Ba^{2+} currents and those of Ca^{2+} currents at 70 mM, clearly showing that the species of ion affects the kinetics of L-VGCC current. Moreover, since the L-VGCC in hair cells showed Ca^{2+}-dependent inactivation, it raises the possibility that damped oscillations in the membrane potential may be derived from recovery kinetics of inactivation.

This work was supported by a grant to E.N.Y. (NIH, NIDCD, R01 DC03828), and A.R.-C. was supported by a fellowship from Consejo Nacional di Ciencia y Technologia/IIE/Fulbright.

REFERENCES

Armstrong, C. E., and W. M. Roberts. 1998. Electrical properties of frog saccular hair cells: distortion by enzymatic dissociation. *J. Neurosci.* 18:2962–2973.

Art, J. J., and R. Fettiplace. 1987. Variation of membrane properties in hair cells isolated from the turtle cochlea. *J. Physiol.* 385:207–242.

Art, J. J., Y.-C. Wu, and R. Fettiplace. 1995. The calcium-activated potassium channels of turtle hair cells. *J. Gen. Physiol.* 105:49–72.

Ashmore, J. F. 1983. Frequency tuning in a frog vestibular organ. *Nature.* 304:536–538.

Chabbert, C. H. 1997. Heterogeneity of hair cells in the bullfrog sacculus. *Pflugers Arch.* 435:82–90.

Church, P. J., and E. F. Stanley. 1996. Single L-type calcium channel conductance with physiological levels of calcium in chick ciliary ganglion neurons. *J. Physiol.* 496:59–68.

Crawford, A. C., and R. Fettiplace. 1981. An electrical tuning mechanism in turtle cochlear hair cells. *J. Physiol.* 312:377–412.

Ertel, A. A., K. P. Campbell, M. M. Harpold, F. Hofmann, Y. Mori, E. Perez-Reyes, A. Schwartz, T. P. Snutch, T. Tanabe, L. Birnbaumer, R. W. Tsien, and W. A. Catterall. 2000. Nomenclature of voltage-gated calcium channels. *Neuron.* 25:533–535.

Fettiplace, R., and P. A. Fuchs. 1999. Mechanisms of hair cell tuning. *Annu. Rev. Physiol.* 61:809–834.

Fox, A. P., M. C. Nowycky, and R. W. Tsien. 1987. Kinetic and pharmacological properties distinguishing three types of calcium currents in chick sensory neurons. *J. Physiol.* 394:149–172.

Fuchs, P. A. 1996. Synaptic transmission at vertebrate hair cells. *Curr. Opin. Neurobiol.* 6:514–519.

Fuchs, P. A., M. G. Evans, and B. W. Murrow. 1990. Calcium currents in hair cells isolated from the cochlea of the chick. *J. Physiol.* 429:553–568.

Guia, A., M. D. Stern, E. G. Lakatta, and I. R. Josephson. 2001. Ion concentration-dependence of rat cardiac unitary L-type calcium channel conductance. *Biophys. J.* 80:2742–2750.

Hagiwara, S., and H. Ohmori. 1982. Studies of calcium channels in rat clonal pituitary cells with patch electrode voltage clamp. *J. Physiol.* 331:231–252.

Hall, J. D., S. Betarbet, and F. Jaramillo. 1997. Endogenous buffers limit the spread of free calcium in hair cells. *Biophys. J.* 73:1243–1252.

Hamill, O. P., A. Marty, E. Neher, B. Sakmann, and F. J. Sigworth. 1981. Improved patch-clamp techniques for high-resolution current recording from cells and cell-free membrane patches. *Pflugers Arch.* 391:85–100.

Hess, P., J. B. Lansman, and R. W. Tsien. 1986. Calcium channel selectivity for divalent and monovalent cations: voltage and concentration

dependence of single channel current in ventricular heart cells. *J. Gen. Physiol.* 88:293–319.

Hille, B. 2001. Ionic Channels In Excitable Membranes. 3rd Ed. Sinauer Associates, Inc., Sunderland, MA.

Hodgkin, A. L., and A. F. Huxley. 1952. A quantitative description of membrane current and its application to excitation and conduction in nerve. *J. Physiol.* 117:500–544.

Hudspeth, A. J., and R. S. Lewis. 1988a. Kinetic analysis of voltage- and ion-dependent conductances in saccular hair cells of the bull-frog, *Rana Catesbeiana*. *J. Physiol.* 400:237–274.

Hudspeth, A. J., and R. S. Lewis. 1988b. A model for electrical resonance and frequency tuning in saccular hair cells of the bullfrog, *Rana catesbeiana*. *J. Physiol.* 400:275–297.

Imredy, J. P., and D. T. Yue. 1994. Mechanism of Ca^{2+}-sensitive inactivation of L-type Ca^{2+} channels. *Neuron.* 12:1301–1318.

Kollmar, R., J. Fak, L. G. Montgomery, and A. J. Hudspeth. 1997a. Hair cell-specific splicing of mRNA for the α_{1D} subunit of voltage-gated Ca^{2+} channels in the chicken's cochlea. *Proc. Natl. Acad. Sci. USA.* 94:14889–14893.

Kollmar, R., J. Fak, L. G. Montgomery, and A. J. Hudspeth. 1997b. Predominance of the α_{1D} subunit in L-type voltage-gated Ca^{2+} channels of hair cells in the chicken's cochlea. *Proc. Natl. Acad. Sci. USA.* 94:14883–14888.

Koschak, A., D. Reimer, I. Huber, M. Grabner, H. Glossmann, J. Engel, and J. Striessnig. 2001. α_{1D} ($Cav_{1.3}$) subunits can form L-type Ca^{2+} channels activating at negative voltages. *J. Biol. Chem.* 25:22100–22106.

Lang, D., and M. Correia. 1989. Studies of solitary semicircular canal hair cells in the adult pigeon. II. Voltage-dependent ionic conductances. *J. Neurophysiol.* 62:935–945.

Lewis, E. R., R. A. Baird, E. L. Leverenz, and H. Koyama. 1982. Inner ear: dye injection reveals peripheral origins of specific sensitivities. *Science.* 215:1641–1643.

Lewis, R. S., and A. J. Hudspeth. 1983. Voltage- and ion-dependent conductances in solitary vertebrate hair cells. *Nature.* 304:538–541.

Mangoni, M. E., T. Cens, C. Dalle, J. Nargeot, and P. Charnet. 1997. Characterization of α-1A Ba^{2+}, Sr^{2+} and Ca^{2+} currents recorded with the ancillary beta 1–4 subunits. *Receptors Channels.* 5:1–14.

Martini, M., M. L. Rossi, G. Rubbini, and G. Rispoli. 2000. Calcium currents in hair cells from semicircular canals of the frog. *Biophys. J.* 78:1240–1254.

Masetto, S., P. Perin, A. Malusà, G. Zucca, and P. Valli. 2000. Membrane properties of chick semicircular canal hair cells in situ during embryonic development. *J. Neurophysiol.* 83:2740–2756.

McNaughton, N. C. L., and A. D. Randall. 1997. Electrophysiological properties of the human N-type Ca^{2+} channel. I. Channel gating in Ca^{2+}, Ba^{2+} and Sr^{2+} containing solutions. *Neuropharmacology.* 36:895–915.

Moser, T., and D. Beutner. 2000. Kinetics of exocytosis and endocytosis at the cochlear inner hair cell afferent synapse of the mouse. *Proc. Natl. Acad. Sci. USA.* 97:883–888.

Nakagawa, T., S. Kakehata, N. Akaike, S. Komune, T. Takasaka, and T. Uemura. 1991. Calcium channel in isolated outer hair cells of guinea pig cochlea. *Neurosci. Lett.* 125:81–84.

Ohmori, H. 1984. Studies of ionic currents in the isolated vestibular hair cell of the chick. *J. Physiol.* 350:561–581.

Platzer, J., J. Engel, A. Schrott-Fischer, K. Stephan, S. Bova, H. Chen, H. Zheng, and J. Striessnig. 2000. Congenital deafness and sinoatrial node dysfunction in mice lacking class D L-type Ca^{2+} channels. *Cell.* 102:89–97.

Roberts, W. M., A. R. Jacobs, and A. J. Hudspeth. 1990. Colocalization of ion channels involved in frequency selectivity and synaptic transmission at presynaptic active zones of hair cells. *J. Neurosci.* 10:3664–3684.

Rodriguez-Contreras, A., and E. N. Yamoah. 2001. Direct measurement of single-channel Ca^{2+} currents in bullfrog hair cells reveals two distinct channel subtypes. *J. Physiol.* 534:669–689.

Rodriguez-Contreras, A., W. Nonner, and E. N. Yamoah. 2002. Ca^{2+} transport properties and determinants of anomalous mole fraction effects of single voltage-gated Ca^{2+} channels in hair cells from bullfrog saccule. *J. Physiol.* 538:729–745.

Safa, P., J. Boulter, and T. G. Hales. 2001. Functional properties of Cav1.3 (α_{1D}) L-type Ca^{2+} channel splice variants expressed by rat brain and neuroendocrine GH_3 cells. *J. Biol. Chem.* 42:38727–38737.

Sidach, S. S., and I. M. Mintz. 2002. Kurtoxin, a gating modifier of neuronal high- and low-threshold Ca^{2+} channels. *J. Neurosci.* 22:2023–2034.

Smith, P. A., F. M. Ashcroft, and C. M. S. Fewtrell. 1993. Permeation and gating properties of the L-type calcium channel in mouse pancreatic β cells. *J. Gen. Physiol.* 101:767–797.

Smotherman, M. S., and P. M. Narins. 1999. The electrical properties of auditory hair cells in the frog amphibian papilla. *J. Neurosci.* 19:5275–5292.

Song, H., L. Nie, A. Rodriguez-Contreras, Z. Sheng, and E. N. Yamoah. 2003. Functional interaction of auxiliary subunits and synaptic proteins with the Ca^{2+} channel ($Ca_V1.3$) may impart hair cell-specific Ca^{2+} current properties. *J. Neurophysiol.* 89:1143–1149.

Spassova, M., M. D. Eisen, J. C. Saunders, and T. D. Parsons. 2001. Chick cochlear hair cell exocytosis mediated by dihydropyridine-sensitive calcium channels. *J. Physiol.* 535:689–696.

Su, Z.-L., S.-C. Jiang, R. Gu, and W.-P. Yang. 1995. Two types of calcium channels in bullfrog saccular hair cells. *Hear. Res.* 87:62–68.

Thibault, O., N. M. Porter, and P. W. Landfield. 1993. Low Ba^{2+} and Ca^{2+} induce a sustained high probability of repolarization openings of L-type Ca^{2+} channels in hippocampal neurons: physiological implications. *Proc. Natl. Acad. Sci. USA.* 90:11792–11796.

Tsien, R. W., D. Lipscombe, D. V. Madison, K. R. Bley, and A. P. Fox. 1988. Multiple types of neuronal calcium channels and their selective modulation. *Trends Neurosci.* 11:431–438.

Wakamori, M., M. Strobeck, T. Niidome, T. Teramoto, K. Imoto, and Y. Mori. 1998. Functional characterization of ion permeation pathway in the N-type Ca^{2+} channel. *J. Neurophysiol.* 79:622–634.

Xu, W., and D. Lipscombe. 2001. Neuronal $Cav1.3_{\alpha1}$ L-type channels activate at relatively hyperpolarized membrane potentials and are incompletely inhibited by dihydropyridines. *J. Neurosci.* 21:5944–5951.

Yamoah, E. N., E. A. Lumpkin, R. A. Dumont, P. J. S. Smith, A. J. Hudspeth, and P. G. Gillespie. 1998. Plasma membrane Ca^{2+}-ATPase extrudes Ca^{2+} from hair cell stereocilia. *J. Neurosci.* 18:610–624.

Yue, D. T., and E. Marban. 1990. Permeation in the dihydropyridine-sensitive calcium channel: Multi-ion occupancy but no anomalous mole-fraction effect between Ba^{2+} and Ca^{2+}. *J. Gen. Physiol.* 95:911–939.

Zagotta, W. N., T. Hoshi, and R. W. Aldrich. 1994. *Shaker* potassium channel gating. III. Evaluation of kinetic models for activation. *J. Gen. Physiol.* 103:321–362.

Zamponi, G. W., and T. P. Snutch. 1996. Evidence for a specific site for modulation of calcium channel activation by external calcium ions. *Pflugers Arch.* 431:470–472.

Zei, P. C., and R. W. Aldrich. 1998. Voltage-dependent gating of single wild-type and S4 mutant KAT1 inward rectifier potassium channels. *J. Gen. Physiol.* 112:679–713.

Zhou, W., and S. W. Jones. 1995. Surface charge and calcium channel saturation in bullfrog sympathetic neurons. *J. Gen. Physiol.* 105:441–462.

Zidanic, M., and P. A. Fuchs. 1995. Kinetic analysis of barium currents in chick cochlear hair cells. *Biophys. J.* 68:1323–1336.